J. Fluid Mech. (2002), *vol.* 453, *pp.* 1–19.
DOI: 10.1017/S0022112001005900 Printed in the United Kingdom

Using surfactants to control the formation and size of wakes behind moving bubbles at order-one Reynolds numbers

By YANPING WANG[1], DEMETRIOS T. PAPAGEORGIOU[1] AND CHARLES MALDARELLI[2]

[1]Department of Mathematical Sciences, and Center for Applied Mathematics and Statistics, New Jersey Institute of Technology, Newark, NJ 07102, USA

[2]Levich Institute and Department of Chemical Engineering, City College of New York, Convent Avenue at 140th Street, New York, NY 10031, USA

(Received 5 June 2000 and in revised form 5 June 2001)

A bubble translating through a continuous liquid (i.e. Newtonian) phase moves as a sphere when inertial and viscous forces are small relative to capillary forces. Spherical bubbles with stress-free interfaces do not retain wakes at their trailing ends as inertial forces become important (increasing Reynolds number). This is in contrast to translating spheres with immobile interfaces in which flow separation and wake formation occurs at order-one Reynolds number. Surfactants present in the continuous phase adsorb onto a bubble surface as it translates, and affect the interfacial mobility by creating tension gradient forces. Adsorbed surfactant is convected to the trailing end of the bubble, lowers the tension there relative to the front, and creates a tension gradient which reduces the surface flow. For low bulk concentrations of surfactant (or if kinetic exchange between bulk and surface is slow relative to convection), diffusion towards the surface is much slower than convection, and surfactant is swept into an immobile cap at the trailing end. As with solid spheres, these caps entrain wakes at order-one Reynolds number. In adsorptive bubble technologies where solutes transfer between the bubble and the continuous phase, usually through thin boundary layers around the bubble surface (high Péclet number), these wakes generally form owing to the presence of surfactant impurities. The wake presence retards the interphase transfer displacing the thin boundary layer towards the front end of the bubble; as mass transfer through the wake is much slower than through the boundary layer, the mass transfer is reduced.

Our recent theoretical research has demonstrated that at low Reynolds numbers, the mobility of a surfactant-retarded bubble interface can be increased by raising the bulk concentration of a surfactant which kinetically rapidly exchanges between the surface and the bulk. At high bulk concentrations the interface saturates with surfactant, effectively removing the tension gradient. In this paper, we demonstrate theoretically that this interfacial control is still realized at order-one Reynolds numbers, and, more importantly, we show that the control can be used to manipulate the formation, size and ultimately the disappearance of a wake. This wake removal mechanism has the potential to dramatically increase the interphase transfer in adsorptive bubble technologies.

1. Introduction

When a gas bubble of radius a, having a clean interface moves with steady velocity U through a continuous liquid phase of density ρ and viscosity μ, by the action of a driving force, the steady flow field, in the absence of inertia, is given by the Hadamard–Rybczynski solution (see Edwards, Brenner & Wasan 1991). For this external creeping flow, the spherical shape is an exact solution that does not have closed streamlines in the region exterior to the bubble, and in particular no wakes at the back end. At finite Reynolds numbers ($Re = \rho Ua/\mu$), inertia can distort the spherical shape and can change the flow field significantly. When inertial forces are small relative to surface tension forces (i.e. the Weber number $We = \rho aU^2/\gamma$ is small where γ is the surface tension coefficient), Moore (1959) has shown that the bubble remains almost spherical for both small and large Reynolds numbers. (See also Moore (1963, 1965) for drag calculations using boundary-layer theory.) Numerical work by Ryskin & Leal (1984) confirms this finding and more importantly shows that the streamlines remain open for Reynolds numbers less than 125 (which was the largest Reynolds number studied); a similar conclusion was obtained by Blanco & Magnaudet (1995) for a wider range of Reynolds numbers less than 500. As We increases, inertia distorts the drop from nearly spherical to oblate-ellipsoidal and spherical cap shapes. At these higher Weber numbers, where the distortion is significant, flow separation and wake formation occur at the back end if the Reynolds number is sufficiently large. In the case where the bubble remains spherical, the absence of a wake at all Reynolds numbers contrasts to the case of a solid sphere where flow separation and wake formation occur at Reynolds numbers larger than about 12 (see Clift, Grace & Weber 1978; Johnson & Patel 1999).

The fact that solid spheres develop wakes at relatively small Reynolds numbers whereas clean spherical bubbles do not (at any Re), suggests that a reduction in a spherical bubble's interfacial mobility can cause a wake to form at its back end. Moreover, if the interfacial mobility can be controlled, the appearance as well as the size of the wake can also be controlled. Such a control can enhance interphase mass transfer in processes where bubbles are forced to rise through a continuous phase in order to extract undesirable components of the gas phase into the liquid (see Huang & Kintner 1969; Beitel & Heideger 1971).

As is well recognized, surfactants adsorbing from the continuous phase onto the bubble interface cause a reduction in interfacial mobility. This reduction arises from the Marangoni forces which develop from the convective partitioning of surfactant as described by Frumkin & Levich (1947), Levich (1962) and Edwards *et al.* (1991). Surfactant adsorbed on the bubble surface is convected by the surface flow from the front to the trailing end. The surface concentration increases causing kinetic desorption into the rear sublayer. This desorption locally raises the sublayer concentration C_s, at the back above the bulk value C_∞, far from the interface. The difference drives a diffusive flux away from the trailing end. Similarly at the front end, the reduction in surface concentration causes kinetic adsorption from the front sublayer onto the front of the bubble. The front sublayer concentration decreases, creating a diffusive flux from the bulk to the front end. Eventually, a steady state develops in which all these fluxes balance. The surface concentration at the trailing end is higher than that at the front, and the interfacial tension γ is lower at the back relative to the front. This interfacial tension difference creates a Marangoni stress along the surface which forces the front part of the surface to tug at the rear, reducing the interfacial mobility and, at steady state, increasing the drag for a given terminal velocity U.

The way the surfactant-induced retardation can give rise to wake formation on a spherical bubble, was first shown by Bel Fdhila & Duineveld (1996) and McLaughlin (1997). Both these studies examined the case in which the exchange of surfactant between the bulk and the surface is much lower than the rate at which surfactant is convected to the back end of the bubble. Scales for the surfactant transport regimes can be constructed as follows. To scale the kinetic rate we use Langmuir kinetics,

$$\beta C_s(\Gamma_\infty - \Gamma) - \alpha\Gamma = j, \tag{1.1}$$

where α and β are the desorption and adsorption rate constants, respectively, j is the kinetic flux, Γ is the surface concentration and Γ_∞ is the maximum packing concentration. For large bulk concentrations, the convective rate is of order $\Gamma_\infty Ua$, where U is the terminal velocity and a the particle radius. As the diffusive rate per unit area is of order DC_∞/a (note that this assumes the diffusion boundary-layer thickness to be of the order of the bubble radius: if the bulk Péclet number Pe – defined below – is large, then the diffusive boundary-layer thickness is of order $aPe^{-1/2}$ for a clean interface and the diffusive rate per unit area is now of order $DC_\infty/aPe^{-1/2}$), where D is the bulk diffusion coefficient, the ratio of diffusive to convective rates can be written as $\chi k/Pe$, where $k = \beta C_\infty/\alpha$, $\chi = \alpha a/\beta\Gamma_\infty$ and Pe is the Péclet number defined as $Pe = Ua/D$. The ratio of kinetic desorption to surface convection is the Biot number, $Bi = \alpha a/U$. In the insoluble limit, we have $\chi k/Pe \ll 1$ or $Bi \ll 1$. Surfactant, therefore, collects at the back end in a stagnant cap while the front end is swept clean of surfactant and is stress-free. In the studies of Bel Fdhila & Duineveld (1996) and McLaughlin (1997) the stagnant cap arose because of the kinetic limitation $Bi \ll 1$ with bulk diffusion rapid, $\chi k/Pe \gg 1$. (This regime was also studied at low Reynolds number by Savic 1953; Griffith 1962; Harper 1973 (for small cap angles); and Davis & Acrivos 1966; Holbrook & Levan 1983*a*; Sadhal & Johnson 1983; He, Maldarelli & Dagan 1991; and Kim & Subramanian 1989*a*.) The order-one Reynolds number studies demonstrated that at sufficiently large Re and cap angles, the immobility of the cap causes a recirculation at the back. In a more complete study in which the stagnant cap arose from slow rates of bulk diffusion and kinetic exchange, Cuenot, Magnaudet & Spennato (1997) showed again the formation of a wake for a spherical bubble at sufficiently high Reynolds number.

These studies illustrate how surfactant can act to form wakes at order-one Re. This stagnant cap regime most commonly arises when surfactant is present at low concentration as an impurity for which the mass transfer limitation gives rise to the cap (i.e. $k\chi/Pe \ll 1$); note that in addition Pe is usually large. The purpose of this study is to examine how surfactants can be used to manipulate the size of the wakes and even cause them to disappear completely. Consider the case in which the kinetic rate is fast relative to convection ($Bi \gg 1$) so that the surface and sublayer are in equilibrium. Bulk diffusion then governs the surfactant transport as given by the magnitude of the parameter $\chi k/Pe$. As this parameter increases to order-one values, diffusive mass transfer becomes of the same order as surface convection and the stagnant cap regime disappears with surfactant spread over the entire bubble surface. In this case, the surface becomes more uniformly retarded rather than completely mobile at the front and solid-like at the back. For low Re, this regime has been studied by several authors for the case $k < 1$. (See Deryagin, Dukhin & Lisichenko 1959; Saville 1973; Levich 1962; Harper 1974; Harper 1982; Levan & Newman 1976; Holbrook & Levan 1983*b*; Chen & Stebe (1996, 1997) for a spherical particle.) As expected, no wakes were observed and the decrease in surface mobility led to an increase in drag. At order-one Reynolds number and $k\chi/Pe = O(1)$, the expected reduced mobility of the

interface could in principle retain the wake created in the stagnant cap regime. This circumstance has not been studied. If in addition the parameter $k\chi/Pe$ becomes large, bulk exchange is much larger than surface convection. This regime was studied for the first time by us at low Re (Wang, Papageorgiou & Maldarelli 1999). It was shown that in this limit the interface is saturated with surfactant leading to a uniform surface concentration, reduction in Marangoni stresses and a return to a tangentially stress-free interface. This remobilization result implies that at order-one Re and $k\chi/Pe \gg 1$, the wake can be removed. Experimentally, the easiest way to set this parameter is to vary the bulk concentration. Thus, at small k, the stagnant cap appears and can cause wake formation. As k increases, the reduced mobility of the surface maintains the wake and finally, at large k, the wake disappears.

The aim of this article is to verify by numerical computations the wake-controlling mechanism surmised above. The model problem and numerical methods are described in § 2. In § 3, we present numerical results of the surface concentration, surface velocity, drag on the bubble and wake structure. In § 4, we make some conclusions and discuss applications to enhancing mass transfer in dispersed phase mass transfer systems. We also give some realistic physical situations where remobilization can be achieved.

2. Mathematical model and numerical methods

Consider a bubble rising through a Newtonian incompressible fluid in an unbounded domain, owing to the action of buoyancy (thermocapillary migration in zero gravity environments is a related problem). The fluid phase contains surfactants, and the dimensionless concentration at any point in space and at time t is denoted by $C(\boldsymbol{x}, t)$. The flow around the bubble is governed by the Navier–Stokes equations and the surfactant concentration satisfies a convection–diffusion equation which couples the hydrodynamics with the transport of surfactant. In addition to the conditions of uniform flow and surfactant concentration at infinity, a set of boundary conditions must be satisfied at the bubble surface (see later). In the present study, we assume that the bubble remains spherical (see § 1) and axisymmetric solutions are sought. We consider a spherical coordinate system, $\boldsymbol{x} = (r, \theta, \phi)$, fixed to the bubble (and centred at the bubble origin), with $\theta = 0$ representing the upstream direction. The corresponding velocity field is defined by $\boldsymbol{u} = (u_r, u_\theta, u_\phi)$. The equations that follow result after the non-dimensionalization discussed in § 1.

Owing to axisymmetry (the solution is independent of the azimuthal angle ϕ), the velocity field can be represented in terms of the Stokes streamfunction ψ as follows:

$$u_r = -\frac{1}{r^2 \sin\theta}\frac{\partial \psi}{\partial \theta}, \qquad u_\theta = \frac{1}{r \sin\theta}\frac{\partial \psi}{\partial r}. \tag{2.1}$$

The corresponding vorticity field is of the form $(0, 0, \omega)$ where

$$\omega = \frac{1}{r}\left[\frac{\partial (r u_\theta)}{\partial r} - \frac{\partial u_r}{\partial \theta}\right] = \frac{1}{r} E^2 \psi, \tag{2.2}$$

where the operator E^2 is given by

$$E^2 \equiv \frac{1}{\sin\theta}\frac{\partial^2}{\partial r^2} + \frac{1}{r^2}\frac{\partial}{\partial \theta}\left(\frac{1}{\sin\theta}\frac{\partial}{\partial \theta}\right). \tag{2.3}$$

The system of equations to be solved, then, becomes

$$\frac{\partial \omega}{\partial t} + \frac{\partial}{\partial r}(r u_r \omega) + \frac{\partial}{\partial \theta}(u_\theta \omega) = \frac{1}{Re} E^2 (r \omega \sin\theta), \tag{2.4}$$

$$\omega = \frac{1}{r}E^2\psi, \tag{2.5}$$

$$\frac{\partial C}{\partial t} + \boldsymbol{u}\cdot\nabla C = \frac{1}{Pe}\nabla^2 C. \tag{2.6}$$

The dimensionless groups appearing in the field equations are the Reynolds number (Re) and the Péclet number (Pe), as defined in § 1.

At this stage, equations (2.4)–(2.6) for the flow and the surfactant concentration are not coupled. Coupling occurs through the boundary conditions on the bubble surface, $r = 1$. The full set of boundary conditions for the hydrodynamics is most conveniently written as

$$\psi = 0 \quad \text{at} \quad \theta = 0, \pi, \tag{2.7}$$

$$\psi = 0 \quad \text{at} \quad r = 1, \tag{2.8}$$

$$\psi = \tfrac{1}{2}r^2 \sin^2\theta \quad \text{as} \quad r \to \infty, \tag{2.9}$$

$$\omega = 0 \quad \text{at} \quad \theta = 0, \pi, \tag{2.10}$$

$$\omega = 0 \quad \text{as} \quad r \to \infty, \tag{2.11}$$

and

$$\omega = \frac{2}{\sin\theta}\frac{\partial \psi}{\partial r}\bigg|_{r=1} + \frac{Ma}{1-\Gamma}\frac{\partial \Gamma}{\partial \theta}, \tag{2.12}$$

where $Ma = RT\Gamma_\infty/\mu U$ is the Marangoni number, and Γ is the dimensionless surface concentration to be found from the concentration field. The boundary condition (2.12) is a statement of tangential stress balance on the bubble surface and use has been made of the Langmuir equation of state which in dimensional form reads

$$\gamma = \gamma_c + RT\Gamma_\infty \ln(1-\Gamma), \tag{2.13}$$

with R, T and γ_c being the gas constant, temperature and clean value of the surface tension, respectively. The Marangoni stress due to surface tension variations on the bubble surface, appears on the right-hand side and its origin is discussed in § 1.

The dimensionless boundary conditions for the surfactant transport equation (2.6) are

$$\frac{\partial C}{\partial \theta} = 0 \quad \text{at} \quad \theta = 0, \pi, \tag{2.14}$$

$$C = 1 \quad \text{as} \quad r \to \infty. \tag{2.15}$$

The boundary condition (2.14) reflects the symmetry and a second condition is required at $r = 1$, which together with the value (2.15) at infinity enables determination of solutions of (2.6). This condition comes from a mass balance of surfactant on the bubble surface, and reads

$$\frac{\partial \Gamma}{\partial t} + \frac{1}{\sin\theta}\frac{\partial}{\partial \theta}(u_\theta \Gamma \sin\theta) = \frac{\chi k}{Pe}\frac{\partial C}{\partial r}\bigg|_{r=1}, \tag{2.16}$$

and relates the surface concentration to the mass flux onto the surface. We note that in (2.16) we have neglected the effects of surface diffusion. For the relatively high values of Pe used in our simulations, the effect of surface diffusion will be negligible in the surface mass transfer. Finally, the equilibrium equation between the surface concentration Γ and the sublayer concentration, provides a nonlinear C–Γ relation on the surface which closes the system; the kinetic exchange relative to surface

convection is very large so that the surface and sublayer are in equilibrium, and it follows from (1.1) that

$$\Gamma = \left.\frac{kC}{1+kC}\right|_{r=1}. \tag{2.17}$$

In equations (2.16) and (2.17), the parameters appearing are given by $\chi = \alpha a/\beta\Gamma_\infty$ and $k = \beta C_\infty/\alpha$ which is a measure of the bulk concentration (see § 1). By substituting the expression (2.17) into the tangential stress balance condition (2.12), the apparent singularity in the latter for $\Gamma = 1$, is seen to be removed.

Owing to the axial symmetry of the flow considered here, the total force acting on the bubble must be in the direction of the axis of revolution, and follows from the total force (we begin using dimensional variables)

$$\boldsymbol{F} = \int \tilde{\boldsymbol{T}} \cdot \boldsymbol{n}\, \mathrm{d}S, \tag{2.18}$$

where $\tilde{\boldsymbol{T}} = -\tilde{p}\boldsymbol{I} + \mu(\nabla\tilde{\boldsymbol{u}} + \nabla\tilde{\boldsymbol{u}}^T)$ is the stress tensor and tildes denote dimensional quantities.

The cumulative effect of the stresses acting over the entire surface of the bubble give rise to a force F_z, say, acting parallel to the axis of revolution where the positive direction is taken to be upstream. It is found from (2.18), then, that

$$\begin{aligned} F_z &= \int_0^\pi \left\{ \left(-\tilde{p} + 2\mu\frac{\partial\tilde{u}_r}{\partial\tilde{r}}\right)\cos\theta - \mu\left[\tilde{r}\frac{\partial}{\partial\tilde{r}}\left(\frac{\tilde{u}_\theta}{\tilde{r}}\right) + \frac{1}{\tilde{r}}\frac{\partial\tilde{u}_r}{\partial\theta}\right]\sin\theta \right\}\Bigg|_{\tilde{r}=a} 2\pi a^2 \sin\theta\, \mathrm{d}\theta \\ &= 2\pi a^2 \int_0^\pi \left(\frac{\sin^2\theta}{2}\frac{\partial\tilde{p}}{\partial\theta} - \frac{\mu}{a}\frac{\partial^2\tilde{\psi}}{\partial\tilde{r}^2}\sin\theta\right)\Bigg|_{\tilde{r}=a} \mathrm{d}\theta \\ &= \pi a^2 \int_0^\pi \sin^2\theta\frac{\partial\tilde{p}}{\partial\theta}\,\mathrm{d}\theta - 2\pi a\mu\int_0^\pi \frac{\partial^2\tilde{\psi}}{\partial\tilde{r}^2}\sin\theta\,\mathrm{d}\theta \\ &= \pi a^2 \int_0^\pi \sin^2\theta\frac{\partial\tilde{p}}{\partial\theta}\,\mathrm{d}\theta - 2\pi a\mu\int_0^\pi \left(\frac{2}{a}\frac{\partial\tilde{\psi}}{\partial\tilde{r}} + \frac{\sin\theta}{\mu}\frac{RT\Gamma_\infty}{\Gamma_\infty - \tilde{\Gamma}}\frac{\partial\tilde{\Gamma}}{\partial\theta}\right)\sin\theta\,\mathrm{d}\theta, \end{aligned} \tag{2.19}$$

where tildes denote dimensional quantities as before.

Making the expression (2.19) dimensionless using inertial scales, yields the drag coefficient, C_D say, experienced by the bubble (it is understood that dependent variables are evaluated at $r = 1$ in the integrals below):

$$\begin{aligned} C_D &= \frac{F_z}{\pi a^2\rho U^2} \\ &= \int_0^\pi \sin^2\theta\frac{\partial p}{\partial\theta}\mathrm{d}\theta - \frac{2}{Re}\int_0^\pi \left(2\frac{\partial\psi}{\partial r} + \frac{Ma\sin\theta}{1-\Gamma}\frac{\partial\Gamma}{\partial\theta}\right)\sin\theta\,\mathrm{d}\theta. \end{aligned} \tag{2.20}$$

The numerical methods used are similar to those described in Wang *et al.* (1999). Briefly, steady-state solutions are obtained by integrating the pseudo-unsteady version of the hydrodynamic equations – this amounts to including a $\partial\psi/\partial t$ term on the left-hand side of (2.5) and integrating the resulting system of parabolic equations forward in time until a steady state is reached (see for example Peyret & Taylor 1983). The time integrations are carried out by using an ADI method which alternates between the r- and θ-directions. For more details, the reader is referred to Wang *et al.* (1999) and Wang (1999).

In the related zero-Reynolds-number problem, the boundary condition for the hydrodynamic problem at infinity can be treated very efficiently by obtaining a

correction to the uniform flow value; the correction depends on the value of the drag on the bubble given by the current iterate, and so imposition of the corrected boundary condition at a finite radial value yields improved accuracy (for details of this see Wang *et al.* 1999). At finite Reynolds numbers, this strategy is no longer tractable analytically and we proceed by applying the boundary condition (2.9) directly at $r = r_\infty$, where r_∞ is sufficiently large and whose value must be checked for accuracy. For example, we performed runs having $r_\infty = 30$ and $Re = 50$ and compared the drag coefficient (non-dimensionalized by the inertial scale $\pi a^2 \rho U^2$) with that obtained from a run having $r_\infty = 20$, and found that the former gives a value which is about 1.5% higher. Runs were also performed on refined grids and we found that the difference between results computed on 50×50 grids with those on 100×100, are less than 2%. In addition, the numerical calculations were checked by determining the drag coefficient without surfactant and the results for $Re = 50$ and our 50×50 grid and $r_\infty = 20$ were within 5% of the numerical calculations of Ryskin & Leal (1984) who found a value of 0.19 and Magnaudet, Rivero & Fabre (1995) who found 0.1845. It is also interesting to compare these results with high-Reynolds-number theories. At $Re = 50$, then, the numerical calculations for clean bubbles are lower than the expression $C_d = 12/Re$ given by Levich (1962) (p. 445), but more accurately given by the corrected expression $C_d = (12/Re)(1 - (2.21/\sqrt{2Re})) = 0.187$ given by Moore (1963).

3. Results

In what follows, we present results from extensive simulations that support our main findings on wake formation and control. We consider results from a computation which varies the surfactant concentration k and the Reynolds number Re, while the Marangoni number, the kinetic parameter χ and the Péclet number, are held fixed at values $Ma = 5$, $\chi = 1$ and $Pe = 100$ and 200. We begin by first illustrating the remobilization of the bubble interface at increasing bulk concentration and at order-one Reynolds numbers. In § 3.1, we show that as the bulk concentration at first increases from zero, surfactant convects and accumulates at the back end. With further increase in bulk concentration, the surface concentration becomes uniform. The surface velocity distributions are given in § 3.2 where we show that as the surface concentration becomes uniform and the Marangoni force disappears, the surface velocity increases towards the clean interface value. In § 3.3, we present results for the drag which show that the reduction in the Marangoni force leads to a reduction in the drag. The effect of the remobilization on the wake formed at the back end is given in § 3.4. In particular, we show that as the bulk concentration increases from zero the Marangoni forces create a significant reduction in interfacial velocity which causes wake formation. Further increase in concentration and the accompanying reduction in Marangoni force (as illustrated in § 3.1–3.3) leads to the disappearance of the wake – these results are illustrated by streamline plots.

3.1. *Surface concentration distributions*

As the bubble moves through the fluid (and a steady state has been reached), surfactant adsorbs onto the surface at the leading edge, is convected to the trailing edge by the surface flow and diffuses into the bulk off the surface. This activity sets up a surfactant gradient on the bubble surface since the concentration is higher at the trailing edge. Numerical solutions depicting typical surface concentration variations with increasing bulk concentration are given in figure 1. The Reynolds number is

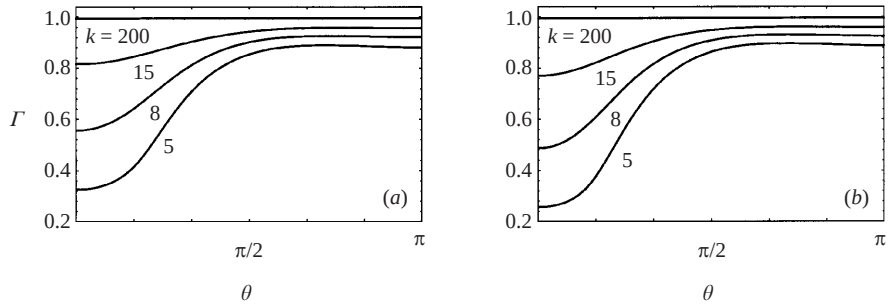

FIGURE 1. The surface concentration distribution, for $Re = 50$, $Ma = 5$ and $\chi = 1$, and $k = \beta C_\infty/\alpha$ is the measurement of bulk concentration. (*a*) $Pe = 100$; (*b*) 200.

$Re = 50$ and two sets of results are shown for Péclet numbers $Pe = 100$ and 200; each set of results is obtained for the values $k = 5, 8, 15$ and 200. It can be seen from the figure that the surface concentration is larger in the vicinity of the trailing edge for any value of k. In addition, when the bulk concentration is relatively small (e.g. $k = 5$), the surface concentration near the front stagnation point is relatively small and has an almost uniform distribution there, while a relatively sharp gradient develops near the rear stagnation point to bring the surface concentration to a much higher and almost uniform value. Such a distribution is typical of the so-called stagnant cap regime which emerges when convection of surfactant on the surface is much larger than diffusion off the surface and into the bulk; the regime is described by the ratio $\chi k/Pe$ being small, as can be surmised from the boundary condition (2.16). The relatively strong surface convection, then, quickly sweeps surfactant to the back end where it accumulates and makes the interface act like a rigid boundary there.

As k increases, the amount of surfactant adsorbed onto the surface increases, as seen from the equilibrium relation (2.17). More importantly, however, the surface concentration gradient decreases with k, and by the time k is increased to 200 the surface concentration gradient is seen to almost disappear and the bubble surface is remobilized. This phenomenon can again be explained by the relative magnitude of the parameter $\chi k/Pe$, which increases as k increases implying that diffusion off the surface and into the bulk at the back end balances surface convection in this limit.

Comparing the surface concentration distributions for $Pe = 100$ and 200, we observe that the larger the Péclet number, the larger the bulk concentration required to remobilize the interface. Another interesting feature to notice is the slight decrease in value of the surface concentration near the rear stagnation point; this is caused by a negative surface velocity at the back end and is discussed in detail in the next section.

3.2. *Surface velocity distributions*

We consider next the velocity distributions on the bubble surface, that is $v_s(\theta) \equiv u_\theta(r = 1, \theta)$. The retardation of the bubble by adsorption of surfactant onto the surface is due to the Marangoni force which is set up by the surface gradients. The surface tension (which is a decreasing function of surface concentration) is lower at the back end than at the front, and the Marangoni force acts from regions of low to high surface tension and so opposes the surface velocity in this case. This retardation is shown in the results of figure 2. In figures 2(*a*) and 2(*b*), we plot the surface velocity, v_s, as a function

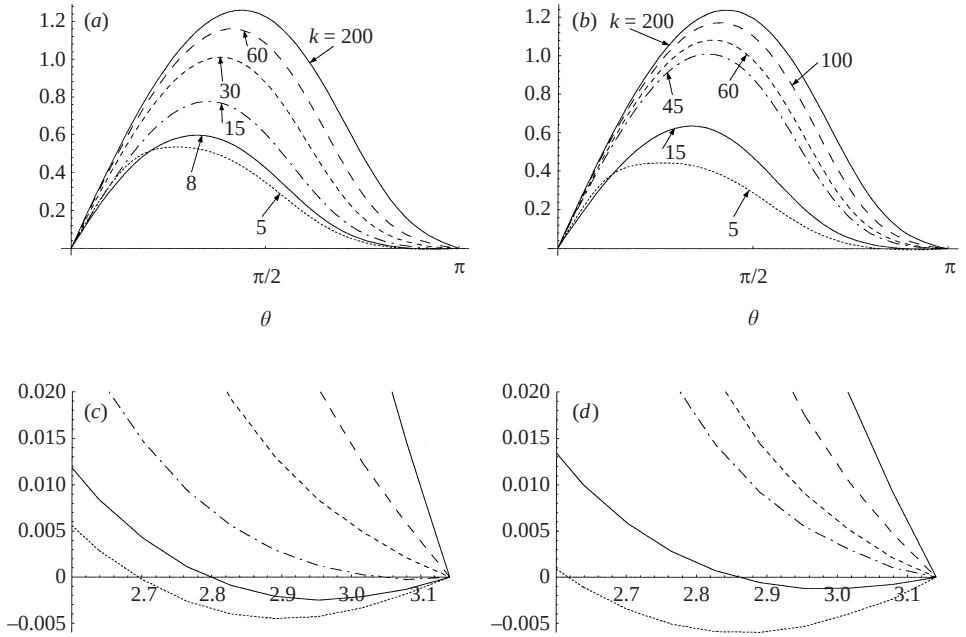

FIGURE 2. Surface velocity, for $Re = 50$, $Ma = 5$ and $\chi = 1$, and $k = \beta C_\infty/\alpha$ is the measurement of bulk concentration. (*a*, *c*) $Pe = 100$; (*b*, *d*) 200.

of θ, for the same values of Reynolds number Re, Marangoni number Ma and χ as used in figure 1, and various bulk concentration values k (shown on the figures), for two different Péclet numbers ($Pe = 100$ and 200). Both sets of computations show that negative velocities are set up in the vicinity of the rear stagnation point for the smaller values of bulk concentration k. Figures 2(*c*) and 2(*d*) depict a magnification of figures 2(*a*) and 2(*b*) respectively, near the rear stagnation point. The first important point to note from figure 2 is that for a fixed Péclet number, the surface velocity increases with k and the velocity profile becomes more symmetric about $\theta = \frac{1}{2}\pi$, corresponding to the fact that the concentrations become more uniform, as shown in figure 1. We also note that when k increases from a value of $k = 5$, the surface velocity near the front stagnation point decreases at first. The reason for this is that as the stagnant cap regime is approached, surfactant convects to the back end by the strong convection after adsorption onto the surface at the front, with small amounts of material left at the front making the surface concentration gradient there small. As k increases, however, a larger surface concentration gradient develops near the front end as the ratio $\chi k/Pe$ becomes larger (but not large enough for remobilization).

Figures 2(*c*) and 2(*d*) show that for the smallest values of k there is a small reversed flow at the back end. The extent of the reversed flow region at the rear as well as the magnitudes of the reversed velocities, are seen to decrease as k increases. This is the first evidence that a wake has formed at the back end of the bubble owing to the retardation of the surface velocity. The fact that for larger values of k this reversed flow disappears validates our claim, as described in § 1, that the appearance of the wake can be controlled by the remobilization of the interface. We also note that this negative velocity pushes surfactant on the surface away from the back stagnation point and causes the small decrease in surface concentration observed in figure 1.

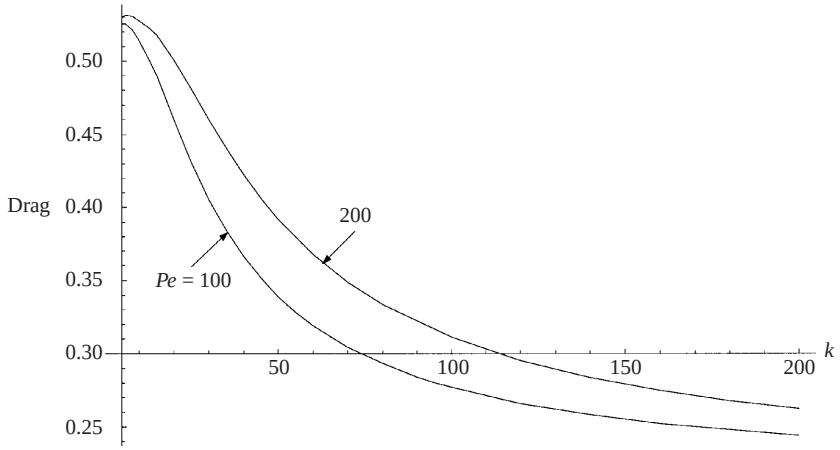

FIGURE 3. The effect of concentration on the drag, for $Re = 50$, $Ma = 5$ and $\chi = 1$, and $k = \beta C_\infty/\alpha$ is the measurement of bulk concentration.

3.3. *Total drag on the bubble*

We consider next, the effect of varying the bulk concentration k on the drag coefficient experienced by the bubble and given by the formula (2.20). We present results for a fixed Reynolds number $Re = 50$ for two different Péclet numbers $Pe = 100$ and 200, the other parameters being fixed as before ($Ma = 5$, $\chi = 1$). The value for the Reynolds number is chosen so that wakes form behind the bubble for relatively low values of k; the bulk concentration k ranges between 5 and 200. Results for the drag coefficient versus k are given in figure 3. As a reference, the drag on a rigid sphere at this Re is 0.55 (see Magnaudet *et al.* 1995) and for a clean spherical bubble it is 0.18 (see Ryskin & Leal 1984; Magnaudet *et al.* 1995). It can be seen that for a fixed Péclet number the drag decreases as the bulk concentration k increases; this corresponds to the increase of the interfacial mobility elucidated in figure 1. The range of k selected is in the regime of remobilization and for smaller values of k the drag rises from the clean bubble value. It is also evident from the results that higher Péclet numbers require a higher value of k to attain a given value of C_D as we have surmised from the fact that $\chi k/Pe$ must become large for remobilization. This is in full agreement with our previous results concerning other flow quantities. We note that the range of k used to produce figure 3 starts at $k = 5$ and as a result the drag coefficient is mostly decreasing – we are at a value of k where remobilization is taking place already. At lower values of k starting from $k = 0$, we observe a monotonic increase of C_D (results not shown). This has been observed in the creeping flow case also (see Wang *et al.* 1999).

3.4. *Wake formation and control*

As already discussed, when convection of surfactant on the bubble surface is larger than the diffusion off the surface (i.e. $\chi k/Pe < 1$), surfactant accumulates at the back and the interface becomes immobile there. This change in the surface boundary condition affects the hydrodynamics globally, and wakes are found to form which would be absent if surfactants were not present, assuming the bubble remains spherical. In fact, we found from our computations that wakes form at order-one Reynolds numbers. This is illustrated in the results of figure 4 which considers the effect of increasing the Reynolds number, all other parameters held fixed. The figure shows the

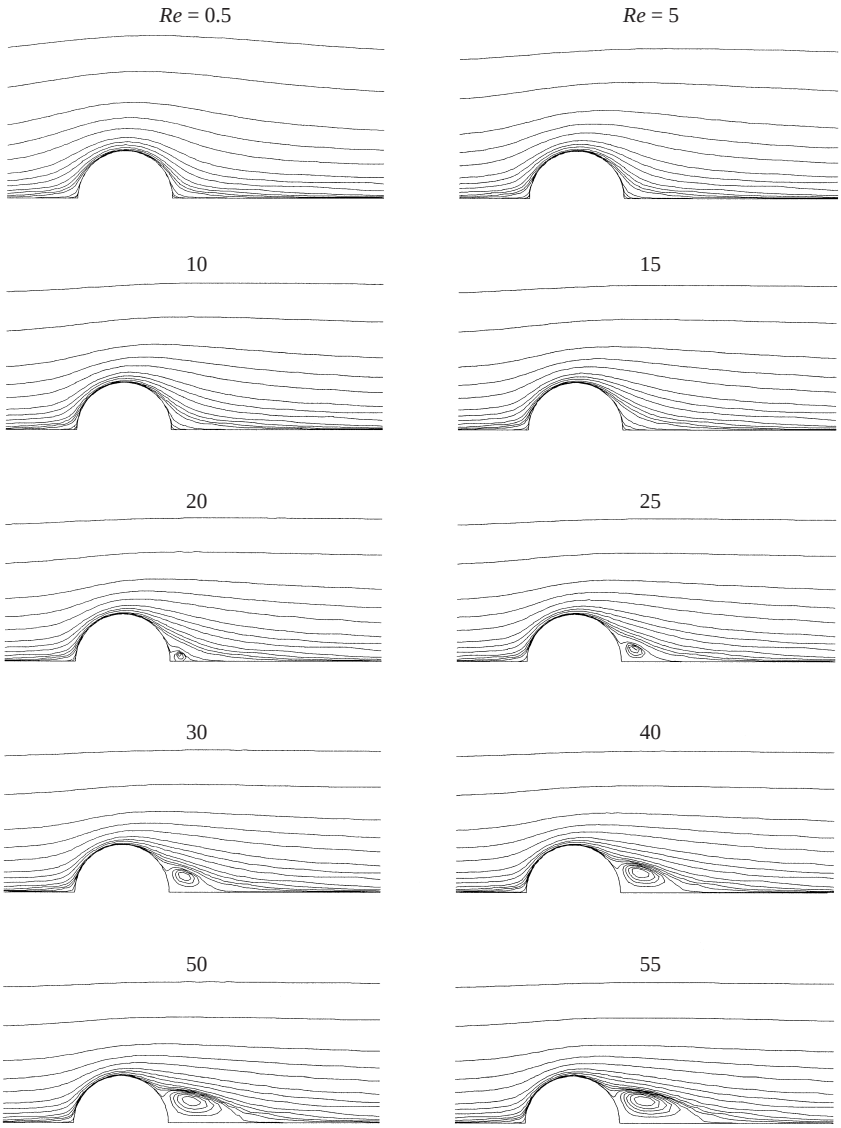

FIGURE 4. Flow around the bubble for $Pe = 100$, $Ma = 5$, $\chi = 1$ and $k = 5$.

streamlines of the flow field (at steady state), for a range of Reynolds numbers – the values of the other parameters in these results are: Péclet number, $Pe = 100$, $k = 5$ (i.e. relatively low bulk concentrations), Marangoni number $Ma = 5$ and $\chi = 1$. For these parameter values, wakes are found to form first at Reynolds numbers between $Re = 15$ and $Re = 20$, which is larger than the corresponding value for a solid sphere which is ($Re \sim 12.5$); as expected the recirculation zone expands as the Reynolds number increases.

Next, we consider the effect of bulk concentration on the flow, at Reynolds numbers which are sufficiently high enough that wakes are formed at low values of k (as in figure 4, for example). To illustrate this, a Reynolds number $Re = 50$ is chosen, the Marangoni number is fixed at $Ma = 5$ and $\chi = 1$. Two different sets of results are presented, the first at $Pe = 100$ and the second at $Pe = 200$. The bulk concentration

is varied by two orders of magnitude with k ranging between values of 5 and 200. Figure 5 is for the run having $Pe = 100$ and figure 6 has $Pe = 200$. Streamline plots are given at steady state as before, which easily enable the identification and relative sizes of recirculating eddies. At the lowest value of $k = 5$ presented, the flow in both figures begins with a relatively large wake whose length is of the order of the bubble diameter. In both cases, an increase in k produces a decrease in the size of the recirculating eddy which eventually disappears when k is big enough. For $Pe = 100$, the wake disappears at a value of k between 25 and 30, whereas for the case $Pe = 200$ this happens at value between 45 and 50. This heralds the remobilization of the bubble by the increase in bulk concentration and the consequent uniformity in surface concentration. It can be seen from figures 5 and 6 that, after remobilization, the streamlines become more symmetric about $\theta = \frac{1}{2}\pi$. We note also that, given the same value of k, the wake has larger dimensions for the higher Péclet numbers. This confirms the results and conclusions of the previous sections (see figures 1 and 2 and the discussion there), since higher Péclet numbers require higher values of k to remobilize the surface.

4. Discussion and conclusions

The calculations presented here demonstrate that surfactants can control the formation and size of wakes behind spherical bubbles moving at order-one Reynolds numbers. The surfactant parameter which describes this control is the ratio of diffusive exchange of surfactant between the bulk and the bubble surface to the surface convection, i.e. $\chi k/Pe$. We have shown that for any order-one Péclet number, when the ratio $\chi k/Pe \ll 1$ and convection outscales exchange, surfactant collects near the rear stagnation point ($\theta = \pi$) making the interface there immobile and allowing wakes to form at order-one Reynolds numbers. The reverse flow near the surface pushes surfactant away from the rear stagnation point towards the front stagnation point, and causes a negative surface velocity near the back end. As k increases, although the amount of surfactant adsorbed onto the surface increases, the surface concentration gradient decreases since the ratio $\chi k/Pe$ increases. The reduction in the surface concentration gradient decreases the Marangoni force and allows the interface to become more mobile. In turn, wakes disappear as the interface near the rear stagnation point becomes more mobile. At $\chi k/Pe \gg 1$, although the total amount of surfactant adsorbed onto the surface is large, the surface concentration becomes uniform (we say the bubble interface remobilizes), as shown in figure 1. In addition to the removal of the wake, the increased mobility of the surface owing to the reduction in the Marangoni force decreases the drag. The larger the Péclet number is the larger the bulk concentration needed to remobilize the bubble interface, as shown in figure 3. For fixed bulk surfactant concentration, the drag increases as the Péclet number increases.

The ability to control the wake behind the bubble has important ramifications in the efficiency of mass transfer operations where solute transfers between a rising bubble and the continuous phase around the bubble. This problem has been of long-standing interest, see for example Clift *et al.* (1978). In bubble mass transfer systems although surfactants are not intentionally added, they are unavoidably present as an impurity in the system. Because of their low concentration, they usually create stagnant caps on the bubble surface which, as we have discussed, can give rise to sizable wakes at the back end. Under the usual case of large Péclet number, the mass transfer picture is as follows. At the front mobile part of the bubble a thin

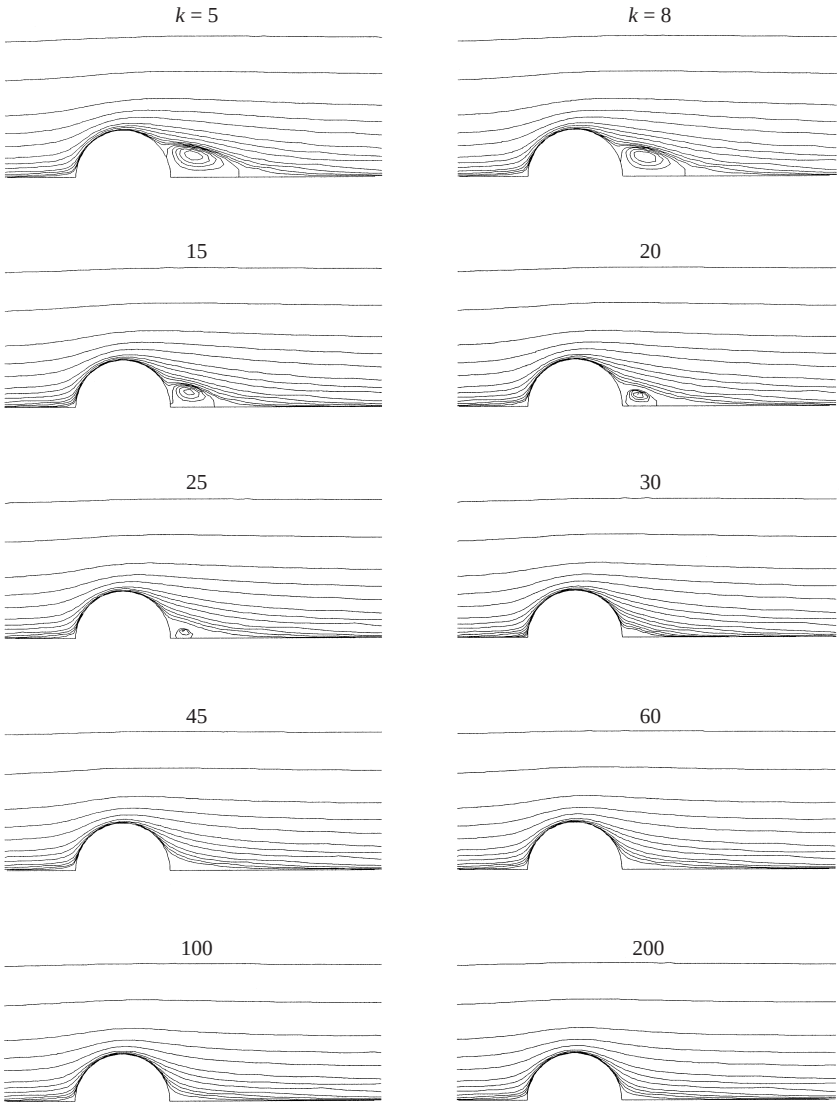

FIGURE 5. Flow around the bubble for $Pe = 100$, $Ma = 5$, $\chi = 1$ and $Re = 50$.

solute boundary-layer thickness of order $Pe^{-1/2}$ is set up implying a flux of order $Pe^{1/2}$. On immobile parts of the surface upstream from the wake, a thin but larger boundary layer of order $Pe^{-1/3}$ also exists. Most of the flux of solute out of the bubble is through these two boundary layers. Finally, solute also diffuses across the slowly recirculating wake. Since the size of this wake is of the order of the bubble radius, the mass transfer is greatly reduced in this region. Thus, the overall effect of the formation of the stagnant cap owing to the surfactant impurity is to significantly reduce the mass transfer rate relative to the case of a clean mobile surface. (The numerical calculations by Takemura & Yabe (1999, see their figure 9) show how drastic this reduction in mass transfer can be.) In this study, we have shown that surfactants which kinetically exchange rapidly between the surface and the liquid sublayer adjacent to the surface, can at high concentration remove the wake by

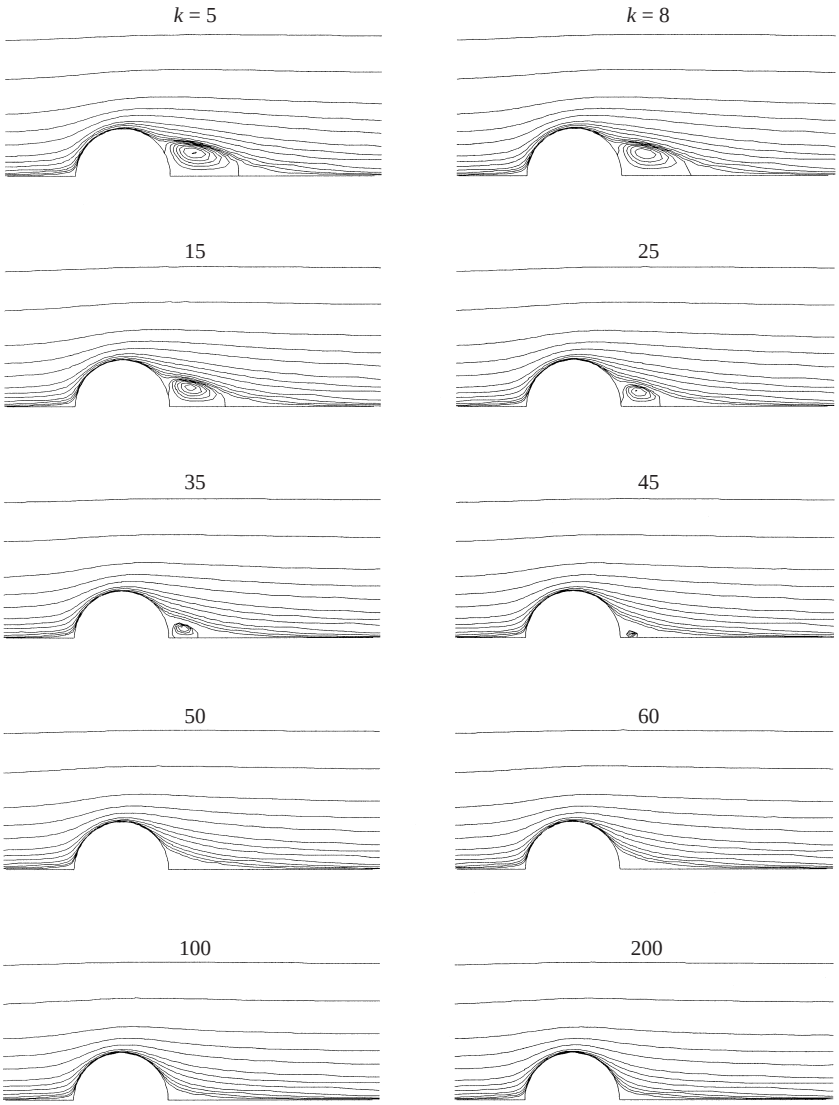

FIGURE 6. Flow around the bubble for $Pe = 200$, $Ma = 5$, $\chi = 1$ and $Re = 50$.

increasing the surface mobility. Therefore, used in mass transfer operations, such surfactants at high concentrations first prevent the impurity from adsorbing and forming a stagnant cap. Secondly, they maintain a high surface mobility along the entire bubble surface which results in an order $Pe^{-1/2}$ solute boundary layer and enhanced mass transfer. We note that the reduction in the solutal boundary-layer thickness will increase the mass transfer even at low Reynolds numbers where wakes are not present.

As a particular physical example, consider the buoyancy-driven motion of a bubble in an aqueous continuous phase. To select a surfactant to remobilize, note the following. Kinetic rate constants are determined by measuring the relaxation in tension as surfactant exchanges between the surface and the bulk. The kinetic constants of only a few systems have been studied (see the review article Chang & Franses 1995);

among them, the medium chain length alcohols have been shown to have relatively large desorption rate constants. The kinetic desorption constant has been measured by Joos & Serrien (1989), for the three to seven chain length alcohols, and found α to be relatively constant and equal to $10^2\,\mathrm{s}^{-1}$. For the common polyethylene oxide surfactants ($C_iE_j(CH_3(CH_2)_{i-1}(OCH_2CH_2)_j - OH)$), measurements by Lin and colleagues (Chang, Hsu & Lin 1998; Lin *et al.* 1996) have shown that the desorption constants are of the order of $10^{-3}\,\mathrm{s}^{-1}$ for $C_{10}E_8$ and $10^{-4}\,\mathrm{s}^{-1}$ for $C_{12}E_8$. We note in fitting the dynamic relaxation data for the polyethoxylates, Lin *et al.* used a Frumkin equation in which the desorption rate had an additional factor of $\exp(K(\Gamma/\Gamma_\infty))$, where $K = 9.6$ for the 10 chain and 5.2 for the 12 chain. The effective desorption rate constant at the high coverage conditions of remobilization is therefore $\alpha\exp(K)$, and hence the effective desorption rate constant is of the order of $14\,\mathrm{s}^{-1}$ for the 10 chain, and $0.05\,\mathrm{s}^{-1}$ for the 12 chain. Thus, from the point of view of satisfying the kinetic constraint, the medium chain alcohols are better candidates than the polyethoxylates. On the other hand, the diffusion limitation requires large bulk concentrations, and this condition favours the polyethoxylates for the following reason. In aqueous solution medium chain length alcohols become insoluble at a limiting concentration, forming a micrometre sized dispersed phase above this concentration. Ethoxylates form aggregates consisting of tens to hundreds of monomers (micelles) at a critical concentration (the CMC); unlike the dispersed insoluble phase of the alcohol, micelles can break down and reform rapidly relative to convective scales. This exchange enhances the transport of surfactant between the surface and the bulk, facilitating remobilization as the concentration of micelles increases. As micelle concentrations can reach high levels before other (slower exchanging) structures form in the phase diagram of the polyethoxylate, micellization can be effective in enabling remobilization for a surfactant whose monomer concentration is not high enough at the CMC to remobilize the interface. However, as the theory detailed in this paper is for concentrations below the CMC, we will restrict our attention to submicellar solutions for polyethoxylates. In table 1, we calculate the transport ratios in an aqueous system for different bubble radii for two surfactants, an alcohol, hexanol and the polyethoxylate with the higher rate constant, $C_{10}E_8$. The insolubility limit for hexanol is $5 \times 10^{-5}\,\mathrm{mole\,cm}^{-3}$, and hence we compute the maximum diffusion/convection transport ratio in the table at this upper limit. The maximum packing concentration, the diffusion coefficient, the equilibrium ratio α/β and the desorption rate constant for hexanol as measured in Joos & Serrien (1989), are $\Gamma_\infty = 6 \times 10^{-10}\,\mathrm{mol\,cm}^{-2}$, $D = 5.2 \times 10^{-6}\,\mathrm{cm}^2\,\mathrm{s}^{-1}$, $\alpha/\beta = 3.7 \times 10^{-6}\,\mathrm{mol\,cm}^{-3}$ and $\alpha = 98\,\mathrm{s}^{-1}$, respectively. The CMC for $C_{10}E_8$ (see Lin *et al.*) is $1 \times 10^{-6}\,\mathrm{mol\,cm}^{-3}$, and this value is used to compute the maximum diffusion/convection ratio for the polyethoxylate. For $C_{10}E_8$ (as measured by Lin *et al.*) the transport values are: $\Gamma_\infty = 3.1 \times 10^{-10}\,\mathrm{mol\,cm}^{-2}$, $D = 6.5 \times 10^{-6}\,\mathrm{cm}^2\,\mathrm{s}^{-1}$, $\alpha/\beta = 1.3 \times 10^{-10}\,\mathrm{mol\,cm}^{-3}$ and $\alpha = 9.7 \times 10^{-4}\,\mathrm{s}^{-1}$. Finally, the characteristic clean bubble velocities (U_{clean}) for the particular bubble radii shown are obtained using the Hadamard–Rybczynski formula ($U_{clean} = \rho g a^2/3\mu$) for low Reynolds number ($Re = \rho U_{clean} a/\mu$) and a correlation for higher Re, $C_D = (8/Re)(1 + 0.15(2Re)^{1/2})$ where C_D is the drag coefficient (defined as $C_D = F_z/(\frac{1}{2}\pi a^2 U_{clean}^2)$) and the correlation is obtained from the numerical simulations in Magnaudet *et al.* (1995).

To have complete remobilization, i.e. a return to an unretarded interface, the parameters Bi and $\chi k/Pe^{1/2}$ (or $\chi k/Pe$, depending on the Péclet number) must be large. The smaller these transport ratios are, the less is the remobilization. In terms of the diffusion limitation, figure 3 for infinite kinetics indicates that when $\chi k/Pe$ (we use

Bubble radius (μm)	U_{clean} (cm s^{-1})	Re	Pe		$Bi = \frac{\alpha a}{U_{clean}}$		$\frac{aC_{max}}{\Gamma_\infty Pe}$ or $\frac{aC_{max}}{\Gamma_\infty Pe^{1/2}}$	
			$C_{10}E_8$	Hexanol	$C_{10}E_8$	Hexanol	$C_{10}E_8$	Hexanol
4×10^2	19	75	1.1×10^5	1.4×10^5	0.03	0.21	0.35	10
10^2	2.5	2.5	3.8×10^3	4.7×10^3	0.06	0.41	0.52	12
10	3.3×10^{-2}	3.3×10^{-3}	4.6	5.8	0.48	3.3	0.57	14
1	3.3×10^{-4}	3.3×10^{-6}	4.6×10^{-3}	5.8×10^{-3}	48	33	80	1.4×10^3

TABLE 1.

the order one in Pe formulation since Péclet numbers in the figure are only of order 100) is equal to approximately 0.3–0.4, the drag is halfway between clean and rigid values, whereas for $\chi k/Pe$ between 2 and 3 the interface is essentially remobilized. To estimate how large a Biot number is necessary for remobilization, we note that Chen & Stebe (1996) calculated the terminal velocities of surfactant-laden bubbles for the case in which the transport is only kinetically controlled. They found that for $Bi = 1$, the terminal velocity is halfway between that of a rigid sphere and a clean bubble, whereas for $Bi = 10$, the interface is essentially remobilized. With these numbers as a guide, it is clear from the table that hexanol will completely remobilize the 1 μm bubbles, and partially remobilize (owing primarily to the kinetic constraint) the 10–400 μm sized bubbles. Most importantly, the wake-controlling mechanism should be realized for bubbles in the size range of 100–400 μm where Reynolds numbers come into the range where wakes can form. The polyethoxylate is only partially remobilizing in the size range of 1–10 μm, and is ineffective at remobilization for the larger bubbles owing to the small Biot numbers (the values of the diffusion parameter would yield partial remobilization in the absence of the kinetic limitation).

The conclusion evident from the table that reduced values of the Biot number represents the primary restriction to remobilization, suggests other hydrodynamic conditions for which these surfactants may be effective at remobilization. If the bubble were a drop with a density close to that of water, then velocities at the same bubble radii would be significantly reduced, and under these conditions the Biot number would be increased (with an increase in the diffusion transport parameter also) and remobilization could be achieved. In addition, if the viscosity of the continuous phase around the bubble were increased from the value of water, the reduced velocity would also increase the Biot number and remobilization should be achieved. In this case, the diffusion transport ratio would not change appreciably from the water values because the reduction in velocity would be compensated by a reduction in the diffusion coefficient of the surfactant in the more viscous continuous phase. Finally, in microgravity conditions, where thermocapillary forces drive the bubble motion, velocities for similarly sized bubbles are much smaller, and hence this type of flow would represent ideal conditions for remobilization. We should note, however, that while reduced velocities will promote conditions for remobilization, the attendant decrease in the Reynolds number may lead to circumstances where wakes are not encountered. One additional point on realizing remobilization in realistic systems is that such systems invariably have impurities which, by themselves, would retard the interface since they are at low concentrations. However, the remobilizing surfactant, because it is present at high concentrations, would not allow the impurities to adsorb when the bubble is created since its adsorption rate would be orders of magnitude larger than the impurity. Thus, remobilization in realistic systems is a two-part mechanism; it protects the interface from retarding impurities as it maintains mobile conditions. In the simulations of this study, Péclet numbers equal to 100 and 200 were used. Although these values are realistic for bubbles with the smaller radii in the table, the associated Reynolds numbers as shown in the table are too low for wake formation. To simulate and illustrate the wake control, the Reynolds number was increased to a value of 50; however, realistic simulations should then take higher values for the Péclet number (since Schmidt numbers in liquids (the product of Pe and Re) are of order 10^3). As these higher values entail special consideration of the diffusion boundary layer for the resolution of the mass transfer, they will be considered in a separate study.

DTP was supported in part by the National Science Foundation (Grant DMS990493), and CM by the National Aeronautics and Space Administration (NASA FAR Award Grant NAG32167).

REFERENCES

Beitel, A. & Heideger,W. J. 1971 Surfactant effects on mass transfer from drops subject to interfacial instability. *Chem. Engng Sci.* **26**, 711–717.

Bel Fdhila, R. & Duineveld, P. C. 1996 The effect of surfactants on the rise of a spherical bubble at high Reynolds and Péclet numbers. *Phys. Fluids* **8**, 310–321.

Blanco, A. & Magnaudet, J. 1995 The structure of the axisymmetric high-Reynolds number flow around an ellipsoidal bubble of fixed shape. *Phys. Fluids* **7**, 1265–1274.

Chang, C. & Franses, E. 1995 Adsorption dynamics of surfactants at the air/water interface: A critical review of mathematical models, data and mechanisms. *Colloids and Surfaces* A **100**, 1–45.

Chang, H., Hsu, C. & Lin, S. 1998 Adsorption kinetics of $C_{10}E_8$ at the air–water interface. *Langmuir* **14**, 2476–2484.

Chen, J. & Stebe, K. 1996 Marangoni retardation of the terminal velocity of a settling droplet: the role of surfactant physico-chemistry. *J. Colloid Interface Sci.* **178**, 144–155.

Chen, J. & Stebe, K. 1997 Surfactant-induced retardation of the thermocapillary migration of a droplet. *J. Fluid Mech.* **340**, 35–60.

Clift, R., Grace, J. R. & Weber, M. E. 1978 *Bubbles, Drops and Particles.* Academic. New York.

Cuenot, B., Magnaudet, J. & Spennato, B. 1997 The effects of slightly soluble surfactants on the flow around a spherical bubble. *J. Fluid Mech.* **339**, 25–53.

Davis, R. E. & Acrivos, A. 1966 The influence of surfactants on the creeping motion of bubbles. *Chem. Engng Sci.* **21**, 681–685.

Deryagin, B. V., Dukhin, S. S. & Lisichenko, V. A. 1959 The kinetics of the attachment of mineral particles to bubbles during flotation. I. The electric field of a moving bubble. *Russ. J. Phys. Chem.* **33**, 389–393.

Edwards, D. A., Brenner, H. & Wasan, D. T. 1991 *Interfacial Transport Processes and Rheology*. Butterworth–Heinemann.

Elzinga, E. R. & Banchero, J. T. 1961 Some observations on the mechanics of drops in liquid–liquid systems. *AIChE J.* **7**, 394–399.

Frumkin, A. & Levich, V. 1947 On surfactants and interfacial motion. *Z. Fiz. Khim.* **21**, 1183 (in Russian).

Griffith, R. M. 1962 The effect of surfactants on the terminal velocity of drops and bubbles. *Chem. Engng Sci.* **17**, 1057–1070.

Happel, J. & Brenner, H. 1973 *Low Reynolds Number Hydrodynamics.* Prentice–Hall.

Harper, J. F. 1973 On bubbles with small immobile adsorbed films rising in liquids at low Reynolds numbers. *J. Fluid Mech.* **58**, 539–545.

Harper, J. F. 1974 On spherical bubbles rising steadily in dilute surfactant solutions. *Q. J. Mech. Appl. Maths* **27**, 87–100.

Harper, J. F. 1982 Surface activity and bubble motion. *Appl. Sci. Res.* **38**, 343–351.

He, Z., Maldarelli, C. & Dagan, Z. 1991 The size of stagnant caps of bulk soluble surfactant on the interfaces of translating fluid droplets. *J. Colloid Interface Sci.* **146**, 442–451.

Holbrook, J. A. & Levan, M. D. 1983*a* Retardation of droplet motion by surfactant. Part I. Theoretical development and asymptotic solutions. *Chem. Engng Commun.* **20**, 191–207.

Holbrook, J. A. & Levan, M. D. 1983*b* Retardation of droplet motion by surfactant. Part II. Numerical solutions for exterior diffusion, surface diffusion, and adsorption kinetics. *Chem. Engng Commun.* **20**, 273–290.

Huang, W. S. & Kintner, R. C. 1969 Effects of surfactants on mass transfer inside drops. *AIChE J.* **15**, 735–744.

Johnson, T. A. & Patel, V. C. 1999 Flow past a sphere up to a Reynolds number of 300. *J. Fluid Mech.* 378, 19–70.

Joos, P. & Serrien, G. 1989 Adsorption kinetics of lower chain alkanols at the air/water interface: the effect of structure makers and breakers. *J. Colloid Interface Sci.* **127**, 97–103.

KIM, H. & SUBRAMANIAN, R. 1989*a* Thermocapillary migration of a droplet with insoluble surfactant, I. Surfactant cap. *J. Colloid Interface Sci.* **127**, 417–430.

KIM, H. & SUBRAMANIAN, R. 1989*b* Thermocapillary migration of a droplet with insoluble surfactant, II. General case. *J. Colloid Interface Sci.* **130**, 112–125.

LEVAN, M. & NEWMAN, J. 1976 The effect of surfactant on the terminal and interfacial velocities of a bubble or drop. *AICHE J.* **22**, 695–701.

LEVICH, V. G. 1962 *Physicochemical Hydrodynamics.* Prentice-Hall.

LIN, S. Y., TSAY, R., LIN, L. & CHEN, S. 1996 Adsorption kinetics of $C_{12}E_8$ at the air–water interface: adsorption onto a clean interface. *Langmuir* **12**, 6530–6536.

MCLAUGHLIN, J. B. 1997 Numerical simulation of bubble motion in water. *J. Colloid Interface Sci.* **184**, 614–625.

MAGNAUDET, J., RIVERO, M. & FABRE, J. 1995 Accelerated flows past a rigid sphere or a spherical bubble. Part 1. Steady straining flow. *J. Fluid Mech.* **284**, 97–135.

MOORE, D. W. 1959 The rise of a gas bubble in a viscous liquid. *J. Fluid Mech.* **6**, 113–130.

MOORE, D. W. 1963 The boundary layer on a spherical gas bubble. *J. Fluid Mech.* **16**, 161–176.

MOORE, D. W. 1965 The velocity of rise of distorted gas bubbles in a liquid of small viscosity. *J. Fluid Mech.* **23**, 749–766.

NADIM, A. & BORHAN, A. 1989 The effects of surfactant on the motion and deformation of a droplet in thermocapillary migration. *Phy. Chem. Hydrodyn.* **11**, 753–764.

PEYRET, R. & TAYLOR, T. D. 1983 *Computational Methods for Fluid Flow*. Springer.

PROBSTEIN, R. F. 1994 *Physico-Chemical Hydrodynamics.* Wiley.

RYSKIN, G. & LEAL, L. G. 1984 Numerical solution of free-boundary problems in fluid mechanics. *J. Fluid Mech.* **148**, 1–17.

SADHAL, S. & JOHNSON, R. 1983 Stokes flow past bubbles and drops partially coated with thin films. Part 1. Stagnant cap of surfactant film – exact solution. *J. Fluid Mech.* **126**, 237–250.

SAVIC, P. 1953 Circulation and distortion of liquid drops falling through a viscous medium. *Natl Res. Counc. Can., Div. Mech. Engng Rep.* **MT-22**.

SAVILLE, D. 1973 The effects of interfacial tension on the motion of drops and bubbles. *Chem. Engng J.* **5**, 251–259.

TAKEMURA, F. & YABE, A. 1999 Rising speed and dissolution rate of a carbondioxide bubble in slightly contaminated water. *J. Fluid Mech.* **378**, 319–334.

WANG, Y. 1999 Theoretical study of bubble motion in surfactant solutions. PhD thesis, New Jersey Institute of Technology.

WANG, Y., PAPAGEORGIOU, D. T. & MALDARELLI, C. 1999 Increased mobility of a surfactant retarded bubble at high bulk concentrations. *J. Fluid Mech.* **390**, 251–270.